Micromagnetic Studies of the Effects of Crystalline Anisotropy on the Remanent Magnetization of Ferromagnetic Nanorings

Gabriel D. Chaves-O'Flynn and Cyrill B. Muratov

Department of Mathematical Sciences, New Jersey Institute of Technology, University Heights, Newark, NJ 07102 USA

Numerical simulations were performed for thin ferromagnetic nanorings with non-negligible anisotropy. In a thin film, the cubic crystalline anisotropy reduces to a four-fold symmetric term favoring magnetization along the $\pm\hat{\mathrm{x}}$ and $\pm\hat{\mathrm{y}}$ directions. Our numerical studies use an extension of the previously proposed algorithm for thin film micromagnetic simulations based on optimal grids for the calculation of the stray field. The relative strength of the magnetostatic energy was varied with respect to the crystalline and exchange energies. The remanent magnetization configurations were obtained for a variety of ring geometries and initial saturation orientations. The magnetocrystalline contribution causes the appearance of distinct domains in the annular structure, resulting in a new variety of magnetization configurations. Based on energetic considerations we provide a classification of possible remanent states.

***Index Terms*—Cobalt nanoelements, ferromagnetic nanorings, magnetic anisotropy, micromagnetic simulations, optimal grids, remanence.**

I. Introduction

In the search for nanoelectronic devices that can be reliably controlled for information storage, Magnetoresistive Random Access Memory (MRAM) has been one of the most promising candidates [1], [7], [23], [19]. Annular ferromagnetic nanostructures have the additional advantage of facilitating flux-closure which reduces stray fields and the interaction between neighboring memory units [2], [22], [23], [20]. Previous analytical and numerical work has demonstrated the thermal stability of flux-closure states in soft ferromagnetic materials with negligible anisotropy [14], [3]. Recent experiments have further allowed the application of circumferential fields by injecting current in the center of the ring using an Atomic Force Microscopy (AFM) tip [21] enabling controlled switching between these states, as well as ones containing 360° walls.

Here, we focus on MRAM proposals where the specific location of a 360° wall on an annulus encodes the bit of information [17]. The existence and stability of 360° walls in uniaxial thin films has been previously demonstrated numerically [16] using an optimal grid discretization for the calculation of the stray field [18]. The dipole-dipole interaction plays an important role in maintaining the integrity of the 360° configurations. Experimentally 360° walls have been observed [9], [10], [2] and they are mostly considered a nuisance in paradigms based on control of independent 180° walls. For annular geometries, 360° degree walls belong to the same topological class as the uniformly magnetized configuration and naturally arise after relaxation from the collision of two independent 180° domain walls of equal winding direction.

In this work, we provide a classification of the remanent states that coexist with the 360° walls. This knowledge is important for MRAM devices for assessing stability of configurations against thermal noise and the proper interpretation of read-out signals. It also informs the strategy needed for faithful recording on the memory bit. We use an analysis of the contributions to the energy to explain the features of the configurations with zero topological degree.

Manuscript received November 06, 2012; revised January 12, 2013; accepted January 14, 2013. Date of current version July 15, 2013. Corresponding author: G. D. Chaves-O'Flynn (e-mail: gchaves@njit.edu).

Color versions of one or more of the figures in this paper are available online at http://ieeexplore.ieee.org.

Digital Object Identifier 10.1109/TMAG.2013.2242449

II. Geometry and Material Parameters

We use the coordinate system represented in Fig. 1 (top left) for describing the magnetization configurations. For thin geometries the magnetization is constrained to the film plane and the unit magnetization $\mathbf{m}$ is reduced to $\mathbf{m} = (m_x, m_y, m_z) = (-\sin\theta, \cos\theta, 0)$, same as in [18]. The ring is assumed to be made of a material with stiffness constant $A = 14 \times 10^{-12}$ J/m, cubic magnetocrystalline anisotropy $K = 9.8 \times 10^4 \mathrm{J/m^3}$ and magnetization saturation $M_s = 1.4 \times 10^6$ A/m characteristic of a cobalt alloy [8].

III. Energetics

The energy $E[\mathbf{m}]$ of a specific magnetization configuration $\mathbf{m}(\mathbf{r}) = \mathbf{M}/M_s$ is obtained from:

$$\frac{2E[\mathbf{m}]}{\mu_0 M_s^2} = \int_V \left(Q m_x^2 m_y^2 + l_{\mathrm{ex}}^2 |\nabla \mathbf{m}|^2\right) d^3r + \frac{2E_D}{\mu_0 M_s^2}, \quad (1)$$

where V is the domain occupied by the material, and we defined the quality factor $Q = (2K)/(\mu_0 M_s^2)$ and the exchange length $l_{\mathrm{ex}} = \sqrt{(2A)/(\mu_0 M_s^2)}$. Since $m_z = 0$, the first three terms of the integral can be rewritten as:

$$\mathcal{E}_{\mathrm{K}} = \frac{Q}{8} \int_V (1 - \cos 4\theta) d^3r, \quad (2)$$

$$\mathcal{E}_{\mathrm{exch}} = l_{\mathrm{ex}}^2 \int_V |\nabla\theta|^2 d^3r. \quad (3)$$

The magnetostatic energy term E_D is obtained from

$$\frac{2E_D}{\mu_0 M_s^2} = \int_{\mathbb{R}^3} \int_{\mathbb{R}^3} \frac{\nabla \cdot \mathbf{m}(\mathbf{r}) \, \nabla \cdot \mathbf{m}(\mathbf{r}')}{4\pi |\mathbf{r} - \mathbf{r}'|} \, d^3r \, d^3r', \quad (4)$$

where $\nabla \cdot m$ is understood distributionally after extending $\mathbf{m}$ by zero to the whole of $\mathbb{R}^3$. It has been demonstrated [11], [5], [6] that for thin films the magnetostatic term reduces to a sum of boundary and bulk terms. The volume dependent terms $V \equiv \Omega \times d$ of the sample are replaced by terms that depend on

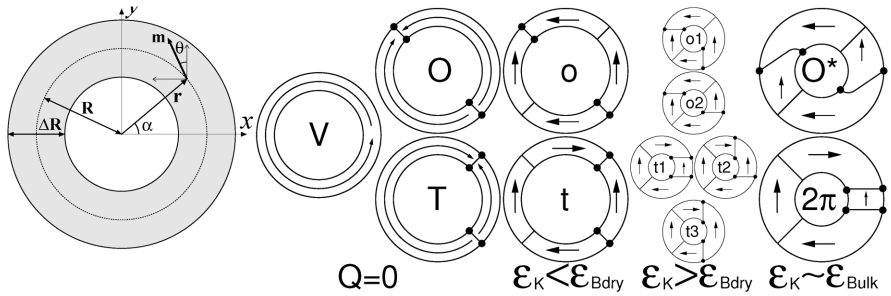

Fig. 1. Far left: Ring geometry. The ring has thickness d, inner and outer radii R_1 and R_2, mean radius $R = (R_1 + R_2)/(2)$, and annular width $\Delta R = R_2 - R_1$. The magnetization vector is in plane and is described by the angle θ with the $\hat{\mathbf{y}}$ direction. The angle α indicates the angle between the radius vector and the $\hat{\mathbf{x}}$ direction. The easy axes point along $\hat{\mathbf{x}}$ and $\hat{\mathbf{y}}$. The rest of the figure: A cartoon representation of the classification of possible distinct remanent states. Here ν decreases from left to right. Domain walls are indicated with lines. Boundary vortices are indicated with dots. Compare with Fig. 2.

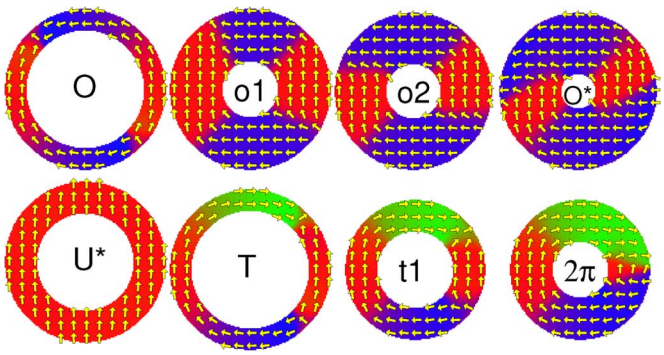

Fig. 2. Remanent states in different rings after saturation by a uniform in-plane field. Top row, from left to right: State O, $R_1 = 12$, $R_2 = 15$, $\nu = 10$, $\theta_0 = 0$; State o1, $R_1 = 6$, $R_2 = 15$, $\nu = 1$, $\theta_0 = (\pi/4)$; State o2, $R_1 = 6$, $R_2 = 15$, $\nu = 2.25$, $\theta_0 = (\pi/4)$; State O*, $R_1 = 4$, $R_2 = 15$, $\nu = 10$, $\theta_0 = (\pi/4)$. Bottom row, from left to right: State U*, $R_1 = 10$, $R_2 = 15$, $\nu = 1$, $\theta_0 = 0$; State T, $R_1 = 12$, $R_2 = 15$, $\nu = 7.75$, $\theta_0 = 0$; State t1, $R_1 = 8$, $R_2 = 13$, $\nu = 5.5$, $\theta_0 = 0$; State 2π, $R_1 = 6$, $R_2 = 13$, $\nu = 7.75$, $\theta_0 = 0$. Each of the figures has been selected as a model for its own class of remanent states. The essential features of these states are described in Fig. 1.

the in-plane region $\Omega \subset \mathbb{R}^2$ and the one-dimensional in-plane boundary $\partial\Omega$

$$\frac{2E_D}{\mu_0 M_s^2} = \mathcal{E}_{\text{trans}} + \mathcal{E}_{\text{bdry}} + \mathcal{E}_{\text{bulk}}. \tag{5}$$

The scaling of the three terms is dramatically different with increasing sample thickness. In (5), the terms have been listed in order of decreasing strength. To the leading order, the first term

$$\mathcal{E}_{\text{trans}} = d \int_\Omega m_z^2 \, d^2 r, \tag{6}$$

strongly penalizes out-of-plane magnetizations justifying the previously stated assumption that $m_z = 0$. The second term

$$\begin{aligned} \mathcal{E}_{\text{bdry}} &= 2\Gamma_{\text{b}} \int_{\partial\Omega} \sin^2(\theta - \alpha)\, ds \\ &\equiv \frac{d^2}{2\pi} \left| \ln\left(\frac{d}{\sqrt{A/K}}\right) \right| \int_{\partial\Omega} \sin^2(\theta - \alpha)\, ds, \end{aligned} \tag{7}$$

penalizes orientations of the magnetization perpendicular to the in-plane boundary; for the annular structures considered here, it favors the so-called vortex configurations. The evaluation of (7) must include both edges of the annulus. Locally, the boundary energy term favors $\theta - \alpha = \pi n$, $n \in \mathbb{Z}$, on $\partial\Omega$, corresponding to the normal component of the magnetization vanishing on the boundary of Ω. However, by topological reasons this is not possible for magnetization configurations with topological degree 0 (recall that the *topological degree* is the winding number of the magnetization vector along any closed loop traced counterclockwise inside the ring). This is in contrast with the for vortex configurations, which have topological degree $+1$. As a consequence, boundary vortices form on either side of the annulus boundary, acting as magnetic point charges in the case of degree 0 magnetization configurations [15], [13]. Finally, the last term

$$\mathcal{E}_{\text{bulk}} \equiv d^2 \int_\Omega \int_\Omega \frac{\nabla \cdot \mathbf{m}(\mathbf{r}) \, \nabla \cdot \mathbf{m}(\mathbf{r}')}{4\pi |\mathbf{r} - \mathbf{r}'|} \, d^2 r \, d^2 r', \tag{8}$$

incorporates magnetostatic interactions in the bulk of the sample. This is the only non-local energy term and accounts for the long-range interactions between walls that may be present in the sample. If the walls are close enough, their mutual attraction results in 360° walls which are robust structures against moderate perturbations coming from other energy contributions. In this work we tune the relative strengths of $\mathcal{E}_{\text{bdry}}$ and $\mathcal{E}_{\text{bulk}}$ by changing the ratio of ΔR to R.

IV. Dynamics

The dynamics of the magnetization may be described by the Landau-Lifshitz equation

$$\frac{\partial \mathbf{m}}{\partial t} = -\gamma(\mathbf{m} \times \mathbf{H}_{\text{eff}} + \alpha_d \mathbf{m} \times (\mathbf{m} \times \mathbf{H}_{\text{eff}})), \tag{9}$$

where γ is the gyromagnetic ratio, α_d is the damping constant and the effective field is given by $\mathbf{H}_{\text{eff}} = -(1)/(\mu_0 M_s)(\delta E)/(\delta \mathbf{m})$. Following [6], [4], [12], the thin film limit version of (9) reduces to a scalar equation for the angle θ

$$\frac{\partial \theta}{\partial t} = \zeta M_s (\mathbf{m} \times \mathbf{h}_{\text{eff}}) \cdot \hat{\mathbf{z}}, \tag{10}$$

with $\zeta \equiv \gamma(\alpha_d + \alpha_d^{-1})$, where $\mathbf{h}_{\text{eff}} = \mu_0 M_s \mathbf{H}_{\text{eff}}/(2K)$.

The computation of the effective field $\mathbf{h}_{\text{eff}}$ in the thin film limit is not straightforward because of the singular nature of different contributions to the magnetostatic energy. To avoid resolving these singularities explicitly, we instead employ a *regularization* by assuming that the magnetization vector extended to the whole plane satisfies a regularized constraint: $|\mathbf{m}(\mathbf{r})| =$

$\chi(\mathbf{r})$, where $\chi(\mathbf{r})$ is a cutoff function which is equal to 1 in the material and decays quickly to zero on the scale of $l_{\rm ex}$ outside the material. Note that χ now encodes the shape of Ω. Introducing the rescalings:

$$\mathbf{r} \to \sqrt{\frac{A}{K}}\,\mathbf{r}, \quad t \to \frac{\mu_0 M_s}{2\zeta K} t, \tag{11}$$

the dynamics of θ can then be shown to reduce to the following equation:

$$\frac{\partial \theta}{\partial t} = \chi^{-1}\nabla\cdot(\chi^2\nabla\theta) - \frac{1}{4}\chi^3 \sin 4\theta - \nu\chi^{-1}(\mathbf{m}\times\nabla\varphi)\cdot\hat{\mathbf{z}}, \tag{12}$$

where now $\mathbf{m} = (-\chi\sin\theta, \chi\cos\theta, 0)$ in $\mathbb{R}^2$ and

$$\varphi(\mathbf{r}) = -\int_{\mathbb{R}^2} \frac{\nabla\cdot\mathbf{m}(\mathbf{r}')}{4\pi|\mathbf{r}-\mathbf{r}'|}\, d^2r'. \tag{13}$$

Here $\nu \equiv (\mu_0 M_s^2 d)/(2\sqrt{AK})$ is the thin film parameter introduced in [18]. Note that for any topological degree 0 configuration the angle θ should be a *continuous* function of $\mathbf{r}$. This condition selects those configurations in our simulations.

V. Remanent Magnetization States

We are interested in finding the co-existing energy minima for a variety of ring dimensions. We integrate (12), starting from the uniform configuration $\theta = \theta_0$. This corresponds to states that have been saturated by a uniform external field which is then removed at time zero. For all cases studied below the unit of length is given by $L = \sqrt{A/K} \approx 12$ nm. In the simulations we fix the material parameters and vary the value of ν by changing d, and also vary R_1, R_2 and θ_0. Varying ν and R_1 changes the relative strengths of different contributions to the energy. Note that other material parameters simply renormalize L and ν, as long as the film thickness does not significantly exceed the exchange length.

We examined two cases for the initial saturation states: in the first case, the initial saturated state is along one of the crystalline easy axes, e.g., $\theta_0 = 0$; in the second case the initial magnetization points along $-\hat{\mathbf{x}} + \hat{\mathbf{y}}$, i.e., in a direction bisecting the easy axes, e.g., $\theta_0 = (\pi/4)$. We let the simulation evolve and record the remanent state. Typical remanent states are shown in Fig. 2 and the features that permit to classify them in different types are shown in Fig. 1. The classification provided is guided by the strength of each energy term in all the regimes considered.

A. Narrow Rings ($\Delta R \ll R$)

This regime was studied extensively and the states found in this regime have been experimentally observed. The magnetization vector aligns closely with the edge and the favored states are known in the literature as vortex (V), onion (O) and twisted (T) states. The initial magnetization configuration does not wind around the annulus and in our model the topological degree of the magnetization configuration is preserved. As a consequence, the vortex configuration is not accessible from the original state. Only the configurations that have topological degree zero are the possible remanent configurations.

For thick rings, $\nu \gg 1$, the dominant term in the energy is $\mathcal{E}_{\rm bdry}$. If the crystalline anisotropy was non-existent, the two isolated charged domain walls in an onion-like configuration could be found in any location in the ring. However, in the presence of four-fold anisotropy the two isolated domain walls travel along the magnetic strip to maximize the area in which the magnetization lies along the crystalline axes. As a result, the walls accommodate to lie at 45° angle from any of the crystalline easy axes. The onion and twisted onion states are the only accessible local energy minima.

While $\mathcal{E}_{\rm bulk}$ and $\mathcal{E}_{\rm exch}$ are still negligible, as ν decreases $\mathcal{E}_{\rm K}$ starts to compete with $\mathcal{E}_{\rm bdry}$. The magnetization starts to deviate from the circumferential direction and aligns more closely with the crystalline axes. While the remanent state still resembles the onion and twisted states the ring now has 4 distinct domains oriented along $\pm\hat{\mathbf{x}}$ or $\pm\hat{\mathbf{y}}$. Two separate 90° walls appear in the vacant locations making 45° angles with the crystalline axes (the other two locations are occupied by 180° walls). Because of their similarity with the previously described states we label these states with lowercase letters (o) and (t).

B. Thinner Films, Wide Rings ($\nu \sim 1, \Delta R \sim R$)

The $\mathcal{E}_{\rm bdry}$ is a singular term that produces a strong penalization at the edges, but inside the circular crown its effect is negligible and the two bulk terms ($\mathcal{E}_{\rm bulk}$ and $\mathcal{E}_{\rm K}$) become the competing terms. For moderately wide rings the penalty by $\mathcal{E}_{\rm bdry}$ becomes less severe and the cores of the charged walls bend towards the crystalline axes. To emphasize this point, we tag with a black circle the tails of the magnetization vectors at the cores of the charged walls in Fig. 1 and show their locations as ΔR increases. Notice that the (o) and (t) state could each become any of several possible states depending on which direction each of the charged walls bends to. As an example, in Fig. 2 we show the states (o1) and (o2) obtained in separate trials of our simulation.

C. Thicker Films, Wide Rings ($\nu \gg 1, \Delta R \sim R$)

If the ring is wide, we have $\mathcal{E}_{\rm K} \gtrsim \mathcal{E}_{\rm bdry}$ and $\mathcal{E}_{\rm bulk} \sim \mathcal{E}_{\rm K}$ for a thicker film. The magnetostatic interaction starts to influence regions where bulk magnetic charges are formed. The interaction between the walls brings them close to each other. It is noticeable that the 90° degree charge free walls remain fixed at their original locations and do not deform. The remanent states found are labeled in Figs. 2 and 1 as (O*) and 2π.

The (O*) is reminiscent of the onion state and its origin can be understood as the natural deformation of the (o2) states for the cases where $\mathcal{E}_{\rm bulk}$ plays a significant role. The core of the walls with boundary vortices make right angles with the inner edge of the annulus and deform as they approach the outer edge so as to reduce the distance with the 90° walls.

The 2π states present distinct 360° walls which are narrower than the state (t1). It should be emphasized that the only energy term which favors the narrowing of the 360° wall is $\mathcal{E}_{\rm bulk}$. The $\mathcal{E}_{\rm bulk}$ term is small locally in a proper regime favors the formation of 360° walls.

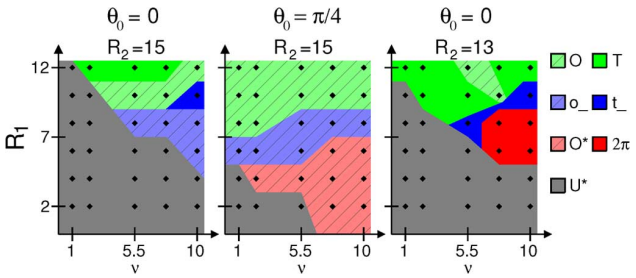

Fig. 3. Final remanent configurations for a variety of physical ring dimensions, using the material parameters in Section II. The (O, T) states and the (o, t) states share the same area in the phase diagram since they transform smoothly into one another without bifurcations as the parameters are changed. The symbol (o_) stands for the region in which either of the (o1, o2) states was the remanent configuration. We have assumed that if (o1) was the remanent state, (o2) would also be a metastable state. In these graphs the actual data points are shown and the region boundaries are drawn by straight line segments.

Similar deformations should exist for cases (o1), (t1), (t2), (t3) although we did not obtain them as remanent states of uniform initial magnetizations. They are not shown in Fig. 1.

D. Thinner Films, Small Holes ($\nu \sim 1, R_1 \ll R_2$)

The parameter ν also carries information about the strength of the exchange energy $\mathcal{E}_{\rm ex}$ relative to the magnetostatic interaction. For moderate ν and rings where the inner hole is very small the ring behaves as a single domain: the ring is uniformly magnetized. However, in the case of non-negligible anisotropy the magnetization, while uniform, can only point in the four possible directions given by the easy axes (state U*).

VI. Coexistence of Remanent States

Fig. 3 summarizes the collection of remanent states for different sizes and ν values. In terms of the physical parameters in Section II the thickness is related to ν by $d \approx \nu \cdot 1$ nm. For $R_2 = 15L$ (≈180 nm) and initial magnetization along the crystalline axis the most likely remanent configuration is the uniform state, the 2π state was not reached. If the initial magnetization is directed at 45° from the crystalline axes, the uniform magnetization is stable only for very small rings. Comparing the results for the two cases where $R_2 = 15L$ coexistence of this states for a variety of parameters is confirmed.

To locate possible parameters for the existence of the 2π state we decrease the outer radius. When R_2 is decreased to $13L$ the 2π state was found in small, wide rings with moderate thicknesses.

VII. Summary

In these proceedings, we have provided a catalogue of states of topological degree zero for rings with significant magnetocrystalline anisotropy. We proposed an energetic interpretation of the features for this family of states. The evaluation of energy barriers between these states is critical to determine thermal stability of magnetic memories, this is the subject of future work. The dynamical behavior of the magnetization close to this set of states can also be studied to understand their resonant modes, which can also be studied experimentally.

Acknowledgment

This work was supported by the NSF via grant DMS-0908279.

References

[1] J. Akerman, "Toward a universal memory," *Science*, vol. 308, no. 5721, pp. 508–510, Apr. 2005.
[2] F. J. Castano, C. A. Ross, C. Frandsen, A. Eilez, D. Gil, H. I. Smith, M. Redjdal, and F. B. Humphrey, "Metastable states in magnetic nanorings," *Phys. Rev. B*, vol. 67, no. 18, p. 184425, May 2003.
[3] G. D. Chaves-O'Flynn, A. D. Kent, and D. L. Stein, "Micromagnetic study of magnetization reversal in ferromagnetic nanorings," *Phys. Rev. B: Cond. Mat. Mater. Phys.*, vol. 79, no. 18, p. 184421, May 2009.
[4] N. Garcia, V. V. Osipov, E. V. Ponizovskaya, and A. del Moral, "Chaotic domain patterns in periodic inhomogeneous magnetic films," *Phys. Rev. Lett.*, vol. 86, pp. 4926–4929, May 2001.
[5] C. J. Garcia-Cervera and W. E. , "Effective dynamics for ferromagnetic thin films," *J. Appl. Phys.*, vol. 90, pp. 370–374, 2001.
[6] C. J. Garcia-Cervera, "One-dimensional magnetic domain walls," *Eur. J. Appl. Math.*, vol. 15, no. 4, pp. 451–486, 2004.
[7] X. F. Han, Z. C. Wen, and H. X. Wei, "Nanoring magnetic tunnel junction and its application in magnetic random access memory demo devices with spin-polarized current switching (invited)," *J. Appl. Phys.*, vol. 103, no. 7, p. 07E933, 2008.
[8] B. Heinrich and J. F. Cochran, "Ultrathin metallic magnetic films: Magnetic anisotropies and exchange interactions," *Adv. Phys.*, vol. 42, no. 5, pp. 523–639, 1993.
[9] M. Klaui, "Head-to-head domain walls in magnetic nanostructures," *J. Phys.: Cond. Mat.*, vol. 20, no. 31, p. 313001, 2008.
[10] M. Klaui, C. A. F. Vaz, L. L. Diaz, and J. A. C. Bland, "Vortex formation in narrow ferromagnetic rings," *J. Phys.: Cond. Mat.*, vol. 15, no. 21, pp. R985–R1024, June 2003.
[11] R. V. Kohn and V. V. Slastikov, "Another thin-film limit of micromagnetics," *Arch. Ration. Mech. Anal.*, vol. 178, no. 2, pp. 227–245, Nov. 2005.
[12] R. V. Kohn and V. V. Slastikov, "Effective dynamics for ferromagnetic thin films: A rigorous justification," *Proc. Royal Soc. A: Math., Phys. Engrg. Sci.*, vol. 461, no. 2053, pp. 143–154, Jan. 2005.
[13] M. Kurzke, "Boundary vortices in thin magnetic films," *Calc. Var. Partial Differ. Eq.*, vol. 26, pp. 1–28, 2006.
[14] K. Martens, D. L. Stein, and A. D. Kent, "Magnetic reversal in nanoscopic ferromagnetic rings," *Phys. Rev. B: Cond. Mat. Mater. Phys.*, vol. 73, no. 5, p. 054413, Feb. 2006.
[15] R. Moser, "Boundary vortices for thin ferromagnetic films," *Arch. Ration. Mech. Anal.*, vol. 174, pp. 267–300, 2004.
[16] C. B. Muratov and V. V. Osipov, "Theory of 360 domain walls in thin ferromagnetic films," *J. Appl. Phys.*, vol. 104, no. 5, pp. 053908–053908-14, Sept. 2008.
[17] C. B. Muratov and V. V. Osipov, "Bit storage by 360 domain walls in ferromagnetic nanorings," *IEEE Trans. Magn.*, vol. 45, no. 8, pp. 3207–3209, 2009.
[18] C. B. Muratov and V. V. Osipov, "Optimal grid-based methods for thin film micromagnetics simulations," *J. Comput. Phys.*, vol. 216, no. 2, pp. 637–653, Aug. 2006.
[19] C. A. Ross and F. J. Castano, "Magnetic Memory Elements Using 360. Degree. Walls," U.S. patent 6906369, Jun. 2005.
[20] C. A. F. Vaz, T. J. Hayward, J. Llandro, F. Schackert, D. Morecroft, J. A. C. Bland, M. Klaui, M. Laufenberg, D. Backes, U. Rudiger, F. J. Castano, C. A. Ross, L. J. Heyderman, F. Nolting, A. Locatelli, G. Faini, S. Cherifi, and W. Wernsdorfer, "Ferromagnetic nanorings," *J. Phys.: Cond. Mat.*, vol. 19, no. 25, p. 255207, Jun. 2007.
[21] T. Yang, N. R. Pradhan, A. Goldman, A. S. Licht, Y. Li, M. Kemei, M. T. Tuominen, and K. E. Aidala, "Manipulation of magnetization states of ferromagnetic nanorings by an applied azimuthal oersted field," *Appl. Phys. Lett.*, vol. 98, no. 24, p. 242505, 2011.
[22] J.-G. Zhu, Y. Zheng, and G. A. Prinz, "Ultrahigh density vertical magnetoresistive random access memory (invited)," *J. Appl. Phys.*, vol. 87, no. 9, pp. 6668–6673, May 2000.
[23] X. Zhu and J.-G. Zhu, "A vertical MRAM free of write disturbance," *IEEE Trans. Magn.*, vol. 39, no. 5, pp. 2854–2856, Sep. 2003.